Nanoprecipitates and Their Strengthening Behavior in Al-Mg-Si Alloy During the Aging Process

HUI LI and WENQING LIU

The different nanoprecipitates formed in a 6061 aluminum alloy during aging at 453 K (180 °C), with or without 168 hours of pre-natural aging (NA), and the age-hardening response of the alloy were investigated by atom probe tomography (APT) and hardness testing. A hardness plateau developed between 2 and 8 hours in both the artificial aging (AA) and artificial aging with pre-natural aging (NAAA) samples. The hardness of NAAA samples was lower than that of AA samples when artificially aged for the same time. A 168-hour NA led to the formation of solute atom clusters in the matrix. The NA accelerated the precipitation kinetics of the following AA. The solute atom clusters gave the highest hardness increment per unit volume fraction. The β'' precipitates were dominant in the samples at the hardness plateau. The average normalized Mg:Si ratios of the solute atom clusters and GP zones were near 1. The average Mg:Si ratio of β'' precipitates increased from 1.3 to 1.5 upon aging for 2 hours. The microstructural evolution of samples with or without NA and its influence on the strengthening effects are discussed based on the experimental results.

DOI: 10.1007/s11661-017-3955-7

I. INTRODUCTION

THE precipitation strengthening 6xxx series Al-Mg-Si alloys are generally used as candidate materials for automobile weight reduction, due to their high strength-to-weight ratios. Solute atom clustering and nanophase precipitation are the key processes in the strengthening of the 6xxx series aluminum alloys.[1–17] A detailed understanding of the dependence of these processes on aging treatment and their influences on strengthening is necessary.

By the increasing use of atom probe tomography (APT) in many recent characterization studies, the growth kinetics,[3,4,10] compositions,[3,4,6,11–13] morphology,[3,4,6,10,13] and number densities[3,4,10,13] of the various precipitates formed in aluminum alloys have been widely investigated at the atomic scale. The precipitation sequence of different precipitates during the aging process is generally accepted as supersaturate solid solution (SSSS), solute atom clusters, Guinier–Preston (GP) zones, metastable β'' precipitates, metastable β' precipitates, and then stable β precipitates.[5,7,13] The different types of precipitates have different strengthening effects. Moreover, the precipitation sequence evolution during artificial aging (AA) with and without pre-natural aging (NA) is different.

Solute atom clusters and GP zones generally precipitate after NA treatment or at the early stage of AA treatment and have significant strengthening effects on the alloys. It is hard to observe them by transmission electron microscopy (TEM), due to their coherent orientation relationship with the matrix and the weak scattering contrast between Mg, Si, and the Al matrix.[2,5–7] The recent emergence of powerful APT has made it possible to visualize the nanoscale precipitates in aluminum alloys.[3–5,9–13] The sizes of solute atom clusters are about 1 to 2 nm, while the sizes of GP zones are somewhat larger than those of the solute atom clusters. The Mg/Si ratios of solute atom clusters and GP zones vary between 1 and 2 in different samples by different characterization methods.[3–7,9–13] Furthermore, the solute atom clusters and GP zones generally happen at room temperature, which is called NA. Natural aging cannot be avoided during practical processing and may have an adverse effect on the age hardening of the subsequent AA treatment.[4,8,9]

Solute atom clusters and GP zones may dissolve into matrix or transform into metastable β'' precipitates during prolonged aging at proper aging temperature. The β'' precipitates with needle shape and 20 to 30 nm in length can obviously be observed in TEM. Thus, the crystal structure of β'' precipitates is well studied in the literature, *e.g.*, References 5,7, and 14 through 17. The composition of β'' precipitates is determined as about Mg_5Si_6 during TEM examination.[5,7,14–17] However, APT results in different reports[5,7,13–17] give many different Mg/Si ratios of β'' precipitates. The compositions of solute clusters, GP zones, and β'' precipitates have strong effects on their following transformation to other types of precipitates.

Other precipitates, such as metastable β' precipitates, stable β precipitates, and so on, generally form in the samples aged for much longer time or at higher temperature. The sizes of these types of precipitates are larger than 50 nm in general.[2,7,18–20] Therefore,

HUI LI and WENQING LIU are with the Key Laboratory for Microstructure, Shanghai University, Shanghai, 200444, P.R. China. Contact e-mail: huili@shu.edu.cn
Manuscript submitted March 27, 2016.
Article published online January 27, 2017

these precipitates are much easier to study by various characterization methods, and more commonly accepted results have been obtained.

So far, the microstructure evolution during the early stage of AA with or without NA in 6xxx series aluminum alloys is still not fully understood and many contradicting results have been reported, such as Mg:Si ratios of solute atom clusters and GP zones, in different literature. Furthermore, the strengthening effects of different precipitates are still not clear. This lack of complete information motivates us to more systematically study the microstructures' evolution and their strengthening effects in a 6061 aluminum alloy.

II. EXPERIMENTAL PROCEDURES

The nominal chemical composition of the as-received sample used in this experiment is 0.82 at. pct Mg, 0.57 at. pct Si, 0.15 at. pct Cu, and balance Al. The samples were solution heat treated at 723 K (550 °C) for 1 hour in vacuum, denoted as SA samples. After solution heat treatment, the samples were subsequently quenched in water. Then the samples were separately heat treated by different processes and denoted as different acronyms:

SA—solution annealing at 723 K (550 °C) for 1 hour, water quenching.

NA—SA and kept at room temperature (293 K (20 °C)) for 168 hours.

AA—SA and directly artificially aged at 453 K (180 °C) for 0 to 128 hours, water quenching.

NAAA—NA and artificially aged at 453 K (180 °C) for 0 to 128 hours, water quenching.

Micro-Vickers hardness measurements were performed using a 50-g load and 10-second dwelling time. At least seven hardness tests were taken for each sample, and then the average results were used to establish the precipitation strengthening curves.

Needle samples for APT analysis were prepared from the sample bars with dimensions of $0.5 \times 0.5 \times 15$ mm^3 using standard two-stage electropolishing.[21] The APT analyses were done under an ultrahigh vacuum (~10^{-8} Pa) at 20 K (−253 °C) and a voltage pulse fraction of 20 pct, using a local electrode atom probe (CAMECA LEAP 4000X HR) and collecting at least 30 million ions for each data set. The evaporation rate is 0.5 pct. The detection rate is about 0.37.

CAMECA IVAS 3.6.8 software was used to do three-dimensional reconstruction and data analyses. The maximum separation algorithm[21] was employed for cluster identification, with Mg, Si, and Cu as clustering solute atoms. The parameters were selected by the following rules: (1) to avoid identifying a single cluster as several clusters, or several small clusters as one larger cluster, a separation distance of 0.7 nm and a surrounding distance of 0.6 nm to include all other elements were selected, according to Figure 1(a); and (2) a minimum cluster size of $n = 10$ was chosen to reduce the effect of small solute clusters that exist in the alloy with solutes in a random distribution. Clusters containing <10 solute atoms were neglected in the analysis, because such small clusters are highly present in a volume with a random distribution of solute atoms.[13,22] These small clusters are unlikely to be responsible for the strength increment observed in the alloy during aging.[13,22]

It is difficult to distinguish clusters, GP zones, β'', and other types of precipitates, due to the lack of crystal structure information in APT data. Different types of precipitates, therefore, were distinguished by their sizes and shapes. Different critical sizes have also been previously used to identify precipitation type in Al alloys in different literature.[13,22–24] In the current research, all solute-enriched features are divided into four groups according to their sizes. Considering a detection efficiency of ~37 pct, a solute atom cluster less than 1.5 nm should be detected containing about 75 atoms of which one third are Al atoms. On this basis, the small solute-enriched features containing 10 to 50 detected solute atoms are designated as solute atom clusters. Those containing 50 to 400 solute atoms are GP zones. Elongated β'' precipitates contain 400 to 5000 solute atoms. Those containing more than 5000 solute atoms are considered to be other precipitates, such as β' and Q' precipitates, and so on. This categorization method can be checked by the shape of the precipitates. It can be seen that the shapes of solute atom clusters are random, GP zones are ellipsoidal, and β'' precipitates are needlelike (Figure 1(b)), which is consistent with the previous literature.[3,4,7,9,13,22]

III. RESULTS

A. *Age-Hardening Response*

The hardness curves of samples during AA and NAAA treatments are shown in Figure 2. A peak hardness of 141 Hv is found at 4 hours in AA sample, while the hardness is only 134 Hv at 4 hours in NAAA sample. The precipitation hardening rate of AA sample is much higher than that of NAAA sample before peak hardness. In contrast, the hardness decrease of AA sample is slower than that of NAAA sample. The hardness decreases to about 100 Hv at 128 hours in both AA and NAAA samples. The general trend of hardness evolution is almost similar to that of many previous reports.[10,13,14,22]

B. *Three-Dimensional Atom Maps*

Figure 3 shows the three-dimensional distribution of solute atoms and their corresponding nearest neighbor distribution (NND) analysis in the SA and NA samples. It seems that Mg, Si, and Cu atoms distribute uniformly in the three-dimensional reconstruction images of the SA samples (Figures 3(a), (c), and (e)), while only small clusters with Mg and Si enrichments can be observed in the NA samples (Figures 3(g), (i), and (k)).

Although the clustering behaviors of solute atoms cannot be observed clearly in the three-dimensional atom maps of the SA and NA samples, the detailed solute atom distributions in the analyzed volume can be revealed by the NND analysis, as shown in Figures 3(b), (d), (f), (h), (j), and (l). The principles of the NND analysis are presented in Reference 25. The NND curves of Mg and Si

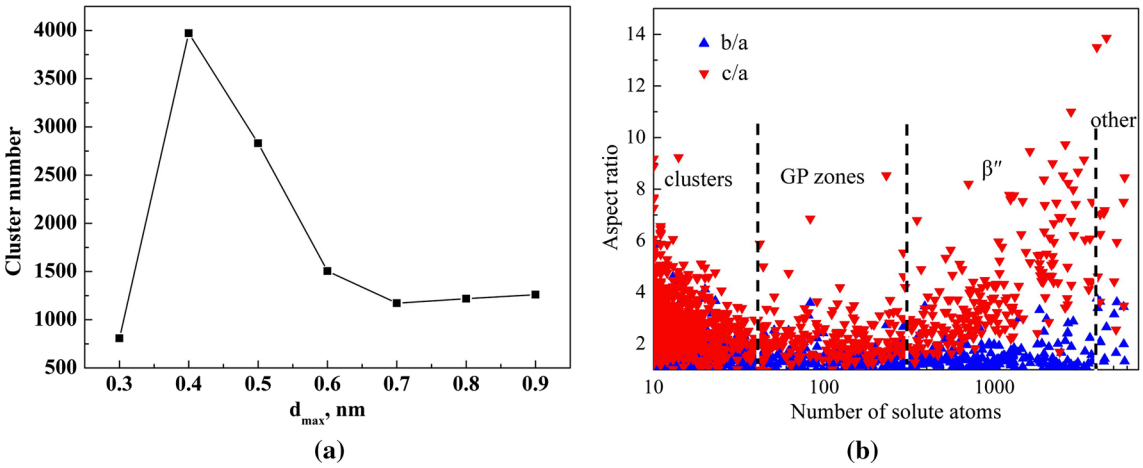

Fig. 1—Analysis methods of solute-enriched features in APT data. (*a*) The dependence of cluster number on the parameter of d_{max}, showing that d_{max} = 0.7 nm can avoid one cluster to be identified as several clusters and randomly distributed solute atoms to be identified as clusters. (*b*) The dependence of the shape of the solute-enriched feature on the number of solute atoms in the precipitate (Color figure online).

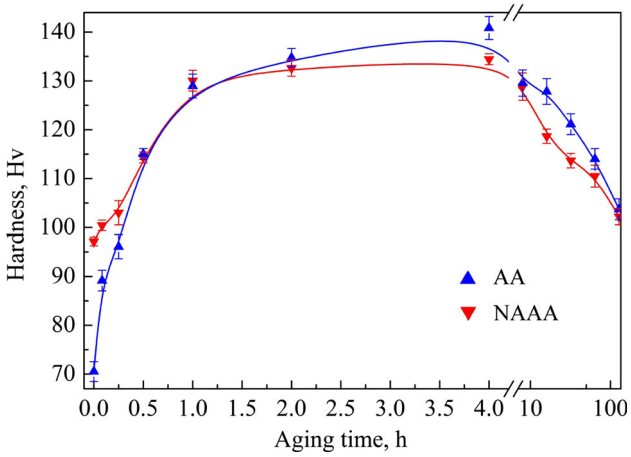

Fig. 2—Microhardness values of AA and NAAA samples (Color figure online).

of the experimental data (black curves) deviate significantly from the NND curves of corresponding random distribution data (red curves) in the SA samples (Figures 3(b) and (d)). This indicates that Mg and Si atoms distribute nonrandomly in the SA samples. In contrast, NND curves of Cu of the experimental data (black curve) and random data (red curve) are very close to each other, indicating that Cu atoms distribute randomly in the SA samples (Figure 3(f)). The NND curves of Mg and Si of the experimental data (black curves) deviate significantly from those of the corresponding random distribution data (red curves) in the NA samples (Figures 3(h) and (j)), which is consistent with the obvious clustering of Mg and Si in their atom maps (Figures 3(g) and (i)). Moreover, NND curves of Cu of the experimental data (black curve) and random data (red curve) are still very close to each other in the NA sample, which indicates that Cu does not take part in the formation of solute atom clusters during NA treatments (Figure 3(l)).

The maximum separation method shows that the numbers of solute atoms in all the solute atom clusters in SA samples are less than 50, and the cluster number density is $1.695 \times 10^{24}/m^3$. The solute atom clusters in SA samples may be formed for the following reasons: (1) the as-quenched samples after solution treatment already contain solute atom clusters,[22] and (2) the NA process takes place and solute atom clusters form during the time (~5 hours) between SA treatment and the APT analysis.[3,4] We think the second reason is dominant for the formation of solute atom clusters shown in Figure 3; it has been shown that 3 hours of NA leads to about 15 Hv increment of the hardness in References 3 and 4, which implies that solute atom clusters form initially in this aging time.

Figures 4 and 5 give the three-dimensional atom maps containing only solute atom-enriched features after removing solute atoms in the matrix of the AA and NAAA samples, respectively. Only small solute atom-enriched features with Mg and Si enrichments can be observed in AA—5 minutes and NAAA—5 minutes samples. These solute atom-enriched features are solute atom clusters and GP zones, because their sizes are less than 3 nm. Only a few needlelike β'' precipitates are evident in the AA—15 minutes and NAAA—15 minutes samples, with an increasing number of solute atom clusters and GP zones. After aging for 2 and 4 hours (peak-aged samples), β'' precipitates are dominant both in AA and NAAA samples. After aging for 8 hours, the precipitates coarsen quickly in the AA and NAAA samples. By comparing the evolution of atom maps, it can be seen that the precipitates in NAAA samples have coarsened more quickly than those in AA samples. The statistical significances of number density, volume fraction, and composition of precipitates in samples aged for more than 8 hours are very low when using APT data. Hence, the following analyses are based on the samples aged for less than 8 hours.

C. *Number Density Evolution of Precipitates*

Figure 6 shows the evolution of the number density of various types of precipitates in the AA and NAAA

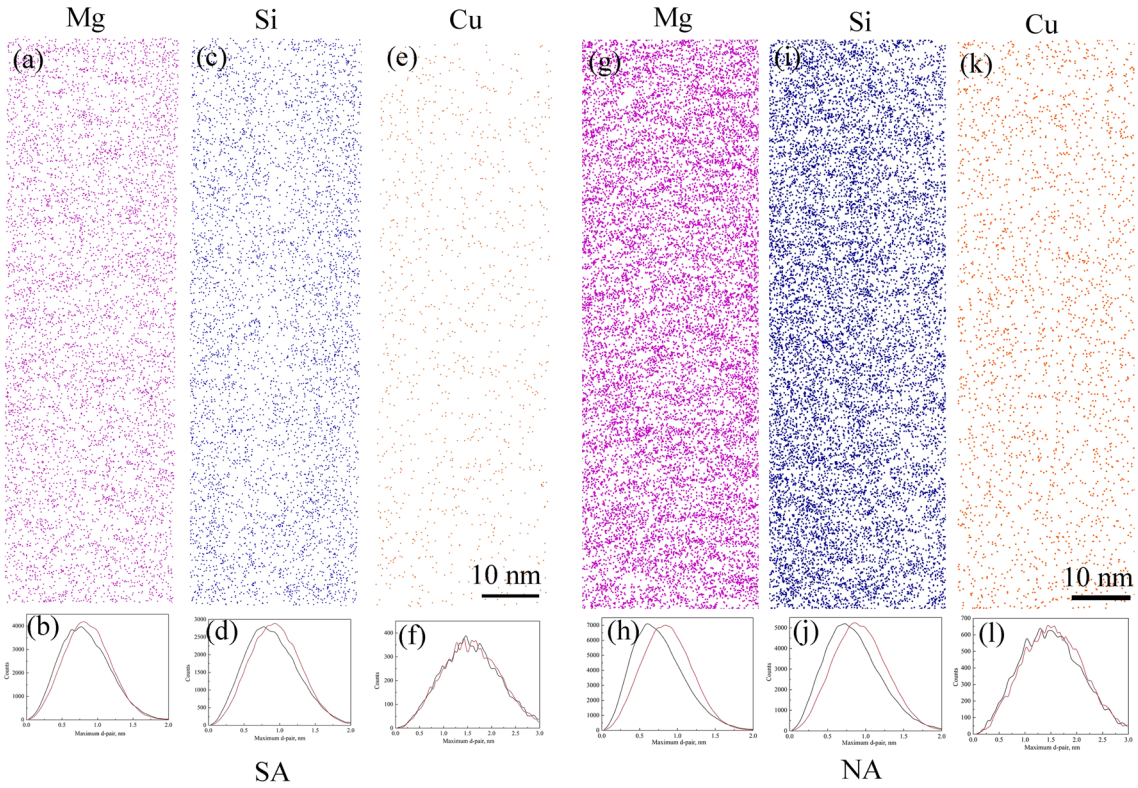

Fig. 3—Three-dimensional atom maps of solute atoms and the corresponding NND curves of (*a*) through (*f*) SA and (*g*) through (*l*) NA samples. The black NND curves are an experimental data set, while the red NND curves are the corresponding reference random distribution data set (Color figure online).

samples during aging for up to 8 hours. The AA—5 minutes sample produces not only high density of solute atom clusters ($1.83 \times 10^{24}/m^3$) and GP zones ($8.20 \times 10^{22}/m^3$), but also a some small β'' precipitates ($1.67 \times 10^{21}/m^3$) (Figure 6(a)). The AA for 15 minutes exhibits a significant increase in the number density of all types of precipitates, and the number density of the solute atom clusters reaches the maximum value ($2.34 \times 10^{24}/m^3$). The number density of GP zones reaches the highest value ($2.38 \times 10^{23}/m^3$) after AA for 30 minutes. Therefore, the number densities of both solute atom clusters and GP zones decrease with prolonged aging time. After AA for 2 to 8 hours, the number density of β'' precipitates increases to the highest value ($1.17 \times 10^{23}/m^3$), while the number density of solute atom clusters decreases to about one sixth of the highest value and that of the GP zones decreases to about half of the highest value (Figure 6(a)). The evolution of β'' precipitate number density is consistent with the hardness curves, as shown in Figure 2.

The evolution of the number density of various types of precipitates in NAAA samples is different from that of AA samples. The NA sample contains a high number density of solute atom clusters ($3.3 \times 10^{24}/m^3$) (Figure 6(b)). Further NAAA for 5 minutes leads to dissolution of solute atom clusters ($2.18 \times 10^{24}/m^3$) and formation of GP zones with low number density of $2.86 \times 10^{22}/m^3$ (Figure 6(b)). The NAAA for 15 minutes leads to a secondary precipitation of solute atom clusters ($2.72 \times 10^{24}/m^3$), and the number density of GP zones reaches the highest value ($2.49 \times 10^{23}/m^3$), as well as the formation of β'' precipitates with low number density ($3.19 \times 10^{22}/m^3$) (Figure 6(b)). Therefore, the number densities of solute atom clusters and GP zones decrease with the prolonged aging time, due to their transformation to β'' precipitates. The NAAA for 2 to 8 hours results in the highest number density of β'' precipitates, more than $1 \times 10^{23}/m^3$, which provides the peak hardness (Figures 2 and 6(b)).

D. *Volume Fraction Evolution of Precipitates*

The evolution of the volume fraction of various types of precipitates in the AA and NAAA samples is shown in Figure 7. The evolution trends of the volume fraction of precipitates in AA and NAAA samples are similar to those of the precipitation number density. The volume fractions of solute atom clusters, GP zones, and β'' precipitates in AA samples reach the highest value at 15 minutes, 30 minutes, and 2 to 4 hours, respectively (Figure 7(a)). The volume fraction of solute atom clusters is highest in the NA aging sample. The volume fraction of solute atom clusters decreases with NAAA for 5 minutes and then reaches another peak value after aging for 15 minutes (Figure 7(b)). The volume fractions of GP zones and β'' precipitates in NAAA samples reach the highest value at 30 minutes and 2 to 4 hours, respectively (Figure 7(b)), which is similar to that of AA samples. By comparing Figures 7(a) and (b), one can see that the volume fractions of solute atom clusters and GP

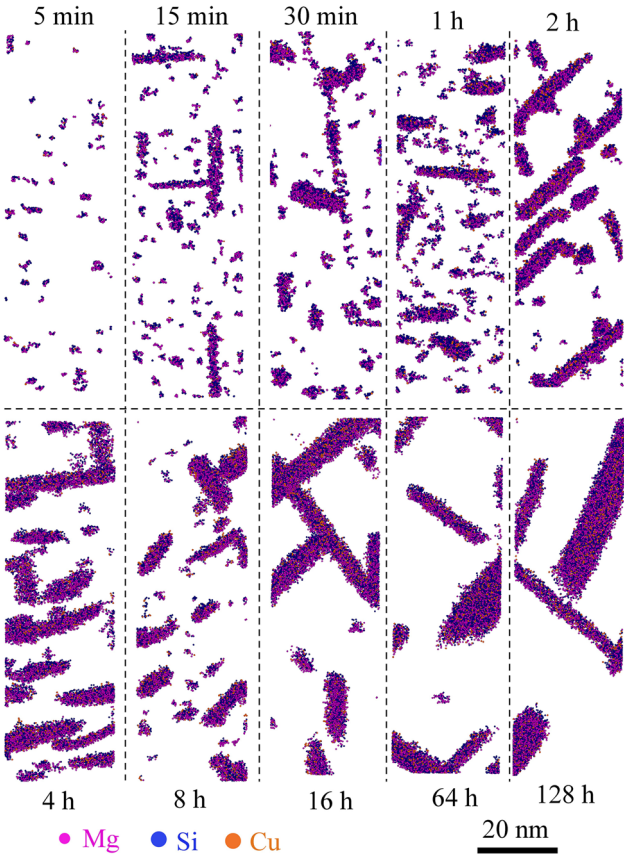

Fig. 4—Three-dimensional atom maps containing only solute atom-enriched features after removal of solute atoms in the matrix of AA samples (Color figure online).

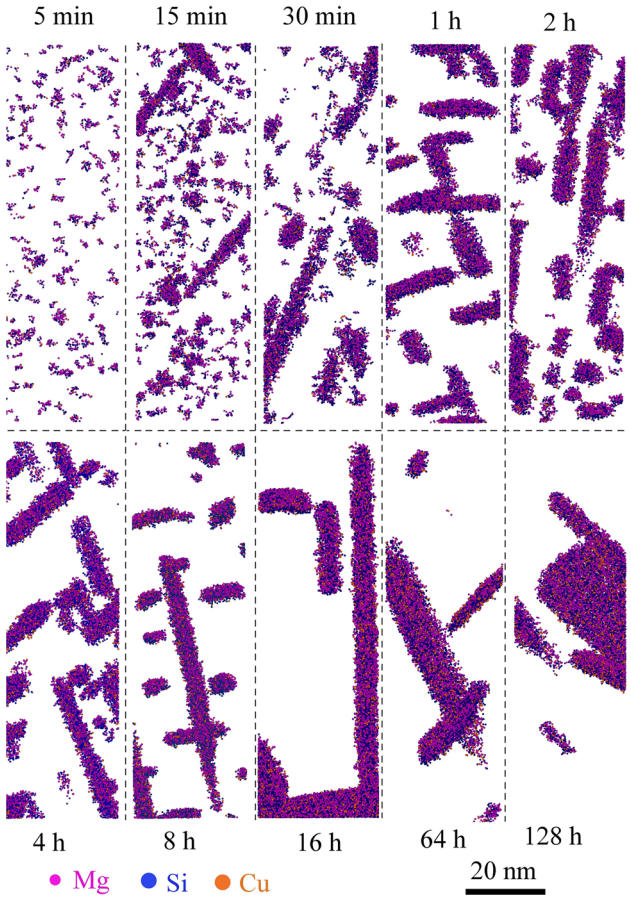

Fig. 5—Three-dimensional atom maps containing only solute atom-enriched features after removal of solute atoms in the matrix of NAAA samples (Color figure online).

zones in NAAA samples are less than those of AA samples after aging for 0.25 hours, while the volume fractions of other types of precipitates in NAAA samples are more than those of AA samples after aging for 0.25 hours.

E. *Chemistry Evolution of Precipitates*

The evolution of the Mg:Si ratios of precipitates in the AA and NAAA samples is shown in Figure 8. The solute atom clusters and GP zones are only solute atoms segregated at the nanoscale, while formation of some new typical phase is not taking place. Therefore, the compositions (Mg:Si ratios) of solute atom clusters and GP zones should be strongly influenced by the composition of bulk alloys. This variation is shown in a number of articles.[5–9,11,13] Thus, the simple calculations of Mg:Si ratios of solute atom clusters and GP zones are not very informative. However, a "normalized Mg:Si ratio," which is independent of matrix composition, can be defined as the Mg:Si ratio of precipitates divided by the Mg:Si ratio of bulk alloys. The normalized Mg:Si ratios of solute atom clusters and GP zones in the AA and NAAA samples are shown in Figures 8(a) and (b), respectively. The β'' and other types of precipitates do have specific crystal structures; their compositions (Mg:Si ratios), therefore, should be less influenced by the composition of bulk alloys. The actual Mg:Si ratios of β'' and other types of precipitates in the AA and NAAA samples are shown in Figures 8(c) and (d), respectively.

The normalized Mg:Si ratios of solute atom clusters and GP zones are similar both in AA (Figure 8(a)) and NAAA (Figure 8(b)) samples, which indicates that the differences of solute atom clusters and GP zones are mainly the size and shape. The normalized Mg:Si ratios of solute atom clusters and GP zones vary only a little around 1 during all the aging treatments, both in AA (Figure 8(a)) and NAAA (Figure 8(b)) samples. This phenomenon shows that most of the solute atom clusters and GP zones are only formed by Mg and Si atoms getting closer to each other, while no Mg enrichment or Si enrichment is dominant. This phenomenon can be concluded from much literature when considering normalized Mg:Si ratios.[5,6,15,23]

The actual Mg:Si ratios of β'' precipitates increase slightly from about 1.3 to about 1.5 before aging for 2 hours, both in AA (Figure 8(c)) and NAAA (Figure 8(d)) samples, which can give some information of the growth process of β'' precipitates. After aging both AA and NAAA samples for 2 hours, the Mg:Si ratios of β'' precipitates stay nearly constant during prolonged aging (Figures 8(c) and (d)), which indicates

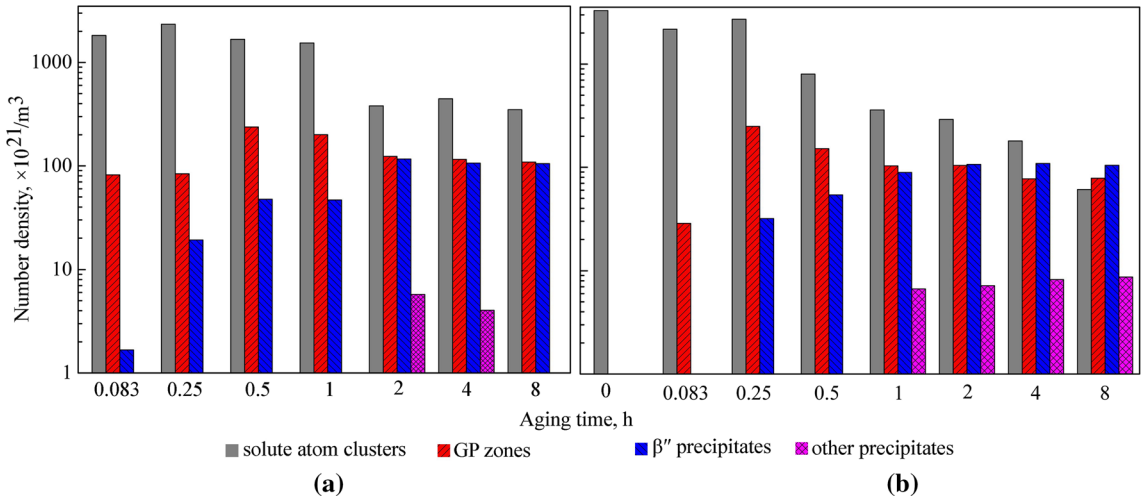

Fig. 6—Evolution of the number density of various types of precipitates in the (*a*) AA and (*b*) NAAA samples (Color figure online).

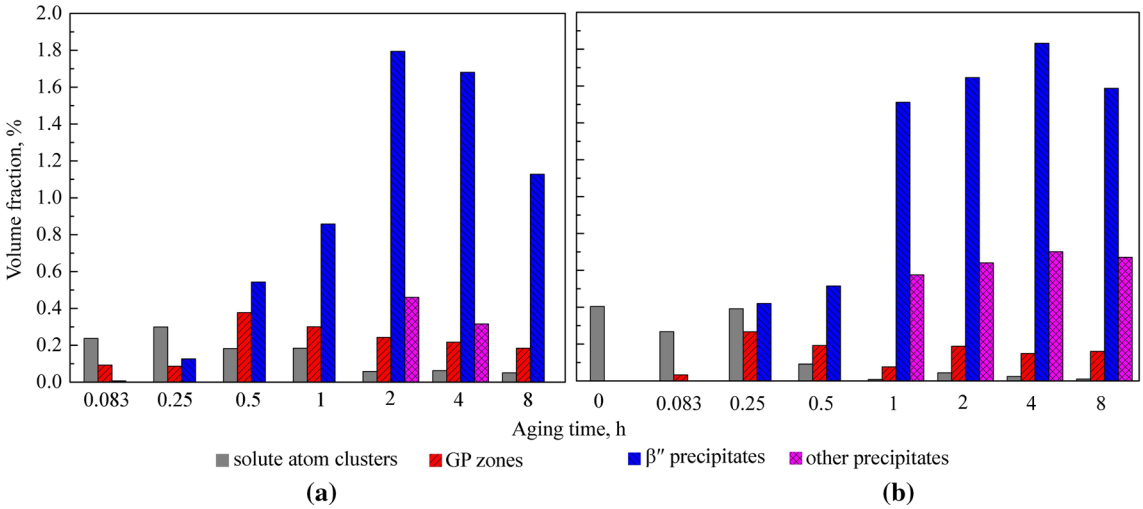

Fig. 7—Evolution of the volume fraction of various types of precipitates in the (*a*) AA and (*b*) NAAA samples (Color figure online).

that the β'' precipitates only grow larger after aging for 2 hours, while their compositions do not change much. The evolution trends of the Mg:Si ratios of other types of precipitates are not possible to analyze from Figures 8(c) and (d), due to the scatter in the data sets.

IV. DISCUSSION

A. *Microstructural Evolution During Aging Treatment*

The different microstructural evolutions of AA and NAAA samples can be derived by comparing Figures 4 through 8. The sizes, shapes, and types of the precipitates evolve continuously without any sharp transition during the aging process.

In AA samples, the evolution trends of number density and volume fraction for various precipitates are different. The peak values of number density and volume fractions of solute atom clusters, GP zones, and β'' precipitates appear at 0.25, 0.5, and 2 hours, respectively, which indicates that the transformation of different precipitates takes place at different aging times. After aging for 2 to 8 hours, the number densities of solute atom clusters, GP zones, and β'' precipitates remain at a steady value, while their volume fractions decrease with prolonged aging. At the same time, the Mg:Si ratio of β'' precipitates reaches a steady value, which indicates that the β'' precipitation is finished after aging for 2 hours. The dissolution of β'' precipitates and transformation to other types of precipitates take place after aging for 4 hours. By comparing Figures 4, 6(a), 7(a), and 8(a) and (c), it can be concluded that different types of precipitates dominate in AA for different times, *e.g.*, SSSS → solute clusters (15 minutes) → GP zones (0.5 hours) → β'' precipitates (2 to 4 hours) → other type precipitates (more than 8 hours).

In NAAA samples, the evolution trends of number density and volume fraction for various precipitates are different, too. However, the microstructural evolutions of NAAA samples have some differences from those of AA samples. The peak values of number density and

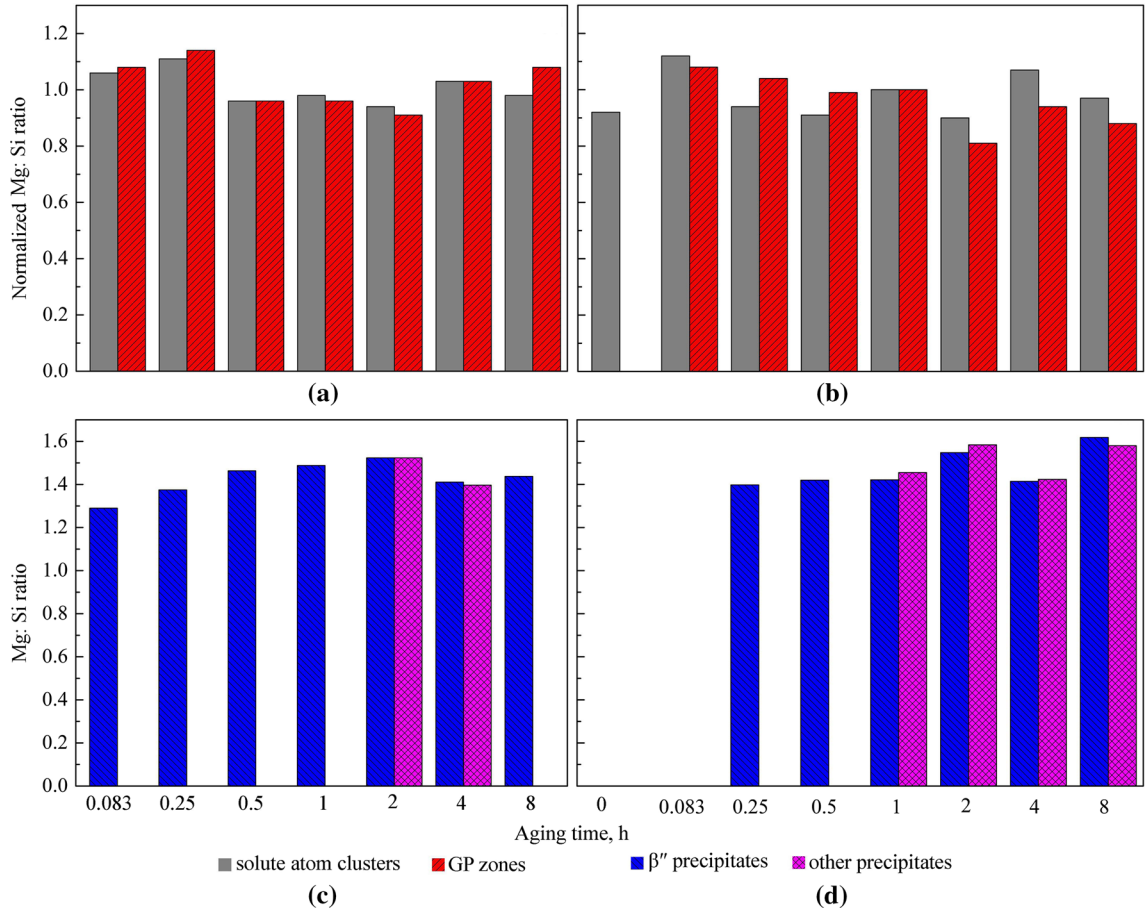

Fig. 8—Evolution of the Mg:Si ratio of various types of precipitates in the (*a*) and (*c*) AA and (*b*) and (*d*) NAAA samples. Normalized Mg:Si ratio means the Mg:Si ratio of the solute atom cluster or GP zone divided by the Mg:Si ratio of the bulk material (Color figure online).

volume fraction of solute atom clusters, GP zones, and β'' precipitates appear at 0.25, 0.25, and 4 hours, respectively. After aging for 4 hours, the number density and volume fraction of solute atom clusters decrease with prolonged aging, which indicates that solute atom clusters transform to other precipitate types. The number densities of GP zones and β'' precipitates remain at a steady value, but their volume fractions decrease with prolonged aging. The Mg:Si ratio of β'' precipitates reaches a steady value after aging for 2 hours, which indicates that β'' precipitation is finished, and transformations to other types of precipitates take place after aging for 4 hours. In summary, different types of precipitates dominate at NAAA for different times (Figures 5, 6(b), 7(b), and 8(b) and (d)), *e.g.*, solute atom clusters I (NA) $\rightarrow$ solute atom clusters II + GP zones (15 minutes) $\rightarrow$ β'' precipitates (2 to 4 hours) $\rightarrow$ other type precipitates (more than 8 hours); while solute atom clusters I is the clusters formed during NA, solute atom clusters II is the clusters formed during NAAA.

B. *Effect of NA on the Following AA*

The main microstructure differences between AA and NAAA samples are the evolution of solute atom clusters and GP zones. Solute atom clusters form easily at the early stage of both NA and AA. Although the solute atom clusters in NA and AA samples generally formed with the assistance of quenched-in vacancies,[26] their formation mechanisms still have some differences. The diffusion rates of Mg (4.9×10^{-27} m^2/s) and Si (1.5×10^{-26} m^2/s) are very slow during NA at room temperature, due to the low temperature.[27] Therefore, the average size of the solute atom clusters is generally very small, while the number densities of the solute atom clusters are very high (Figure 6(b)). The diffusion rates of Mg (1.9×10^{-19} m^2/s) and Si (3.8×10^{-19} m^2/s) are faster during AA at 453 K (180 °C), due to the higher temperature.[27] Then the solute atom clusters grow or transform into GP zones more easily. Therefore, the average size of the solute atom clusters is much larger, while the number densities of the clusters are lower (Figure 6(a)).

The pre-NA has strong influence on the solute atom cluster precipitation during the following AA. The solute atom clusters formed during NA consume most of the quenched-in vacancies, which can assist the formation of new solute atom clusters.[26] The number density of solute atom clusters decreases from 3.3×10^{24}/m^3 in the NA sample to 2.18×10^{24}/m^3 in the NAAA—5 minutes sample (Figure 6(b)). Compared with their volume fraction variations (Figure 7(b)), this

shows that the average size of solute atom clusters in the NAAA—5 minutes sample is somewhat larger than that of the NA sample, which indicates that during the initial stage of NAAA, the solute atom clusters I formed during NA dissolve into the matrix and then another type of solute atom clusters II form in the samples. From the preceding illustration, we observe the dissolution of solute atom clusters I formed during NA indirectly. The dissolution of solute atom clusters I and precipitation of solute atom clusters II further consume the quenched-in vacancies in the sample.

The pre-NA accelerates the precipitation process of AA. The formation possibility of solute atom clusters II in NAAA samples is prohibited, due to fewer quenched-in vacancies existing in the sample. Hence, the number density and volume fraction of solute atom clusters in NAAA samples after the number density peak decrease much more quickly than those of direct AA samples (Figure 6). This leads to quicker precipitation and coarsening of GP zones and faster transformation of the GP zones into other types of precipitates. Hence, after the number density peak, the number densities of GP zones and other types of precipitates in NAAA samples are lower than those of AA samples, while the volume fractions of GP zones and other types of precipitates in NAAA samples are higher than those of AA samples (Figures 6 and 7).

C. *Strengthening Effect of Different Precipitates*

Different types of the precipitates have different strengthening effects on the alloy. In the literature,[6,13,14,19] it is generally simply considered that β'' precipitates have the best strengthening effects, due to the β'' precipitates dominating at the peak hardness (Figures 2 through 7). However, we cannot say that the β'' precipitates have the best strengthening effects. The different types of precipitates mixing in the matrix and having complex interactions with each other result in complex strengthening effects. According to the literature, β'' and other relevant precipitates remain shearable by dislocation through the peak aged condition.[28] Further, the strengthening mechanisms of all types of precipitates are similar, *e.g.*, in terms of order strengthening and modulus hardening.[29–31] Therefore, the different strengthening effects of different precipitates are mainly due to their combined effects of size, number density, volume fraction, average distance of precipitates, and so on.

The solute atom clusters reach the highest number density ($3.3 \times 10^{24}/m^3$) at the initial precipitation strengthening and are falsely thought of as weak strengthening effects precipitates. The small volume fraction (0.40 pct) of solute atom clusters in NA sample gives a raise of more than 26.7 Hv in hardness (Figures 2 and 7). In contrast, the peak volume fraction of β'' precipitate in AA sample (1.79 pct) is nearly 4.5 times the volume fraction of solute atom clusters in NA sample, while it only gives a raise of less than 70.3 Hv in hardness (Figures 2 and 7). Therefore, it can be concluded that the solute atom clusters have the best strengthening effects and β'' precipitates have the weakest strengthening effects when considering unit volume fraction. On the other hand, the solute atom clusters have the weakest strengthening effects and β'' precipitates have the best strengthening effects with respect to the unit precipitation particle, due to the precipitation sizes and number densities. The GP zones have middle strengthening effects considering either unit volume fraction or unit precipitation particle.

The strengthening effects of solute atom clusters and GP zones can be discussed together, because their only difference is the size. The solute atom clusters and GP zones are solute atoms segregated at nanoscale in the matrix, while the crystal structure does not change. The stress fields near the solute atom clusters and GP zones act as weak obstacles of dislocation migration, due to their tiny sizes.[28–31] However, the larger number density of solute atom clusters and GP zones leads to the fact that the distances between the solute atom clusters or GP zones are very small, *e.g.*, only a few nanometers. Hence, the dislocations will meet obstacles with high frequency during migration, and then the solute atom clusters and GP zones will have very high strengthening effects. However, their strengthening effects are limited by the drawback that the volume fractions of solute atom clusters and GP zones can not reach very high values, due to their unavoidable transformation into other types of precipitates during aging.

The β'' precipitates have a different crystal structure and coherent orientation relationship with the matrix. The dislocations have more difficulty shearing one β'' precipitate than one solute atom cluster or one GP zone. Furthermore, β'' precipitates are dominant at the hardness plateau. Therefore, β'' precipitates are generally known as the best strengthening phase when considering per unit number density. However, the low number densities of β'' precipitates indicate that the distances from each β'' precipitate to the next are too far, *e.g.*, dozens of nanometers. If the sample contains β'' precipitates, GP zones, and solute atom clusters with the same volume fraction, the dislocations will meet fewer β'' precipitate obstacles than the solute atom cluster or GP zone obstacles during migration. Therefore, it can be concluded that the β'' precipitates have lower strengthening effects when considering per unit volume fraction.

It is interesting that the volume fractions of β'' precipitates in NAAA samples are higher than those of AA samples during hardness plateaus, while the hardnesses of NAAA samples are lower than those of AA samples (Figures 3 and 7). The average distance between each β'' precipitate in NAAA samples is farther than that in AA samples, due to the lower number densities of β'' precipitates in NAAA samples (Figure 6). The dislocations will meet fewer obstacles during migrating in NAAA samples than in AA samples. Then the hardness of NAAA samples is lower than that of AA samples. Hence, the quicker coarsening of different types of precipitates in NAAA samples is the main reason for the lower hardness of NAAA samples than AA samples.

V. CONCLUSIONS

Based on the experimental results and discussion presented in this article, the following conclusions can be drawn:

1. In the current alloy aged at 453 K (180 °C), the precipitation sequence is continuous while no sharp phase transitions occur at typical aging time. The different types of precipitates dominate at different aging times and can be expressed as SSSS → solute clusters (15 minutes) → GP zones (0.5 hours) → β'' precipitates (2 to 4 hours) → β' and other precipitates (more than 8 hours) in direct artificial samples, and solute atom clusters I (NA) → solute atom clusters II (15 minutes) + GP zones (15 minutes) → β'' precipitates (2 to 4 hours) → β' and other precipitates (more than 8 hours) in samples with NA.
2. The NA accelerates the coarsening of precipitates. The quicker coarsening of different types of precipitates in the samples with NA is the main reason for its lower hardness than direct AA samples.
3. The solute atom clusters have the best strengthening effects, while β'' precipitates have the least strengthening effects when considering per unit volume fraction. In contrast, the solute atom clusters have the least strengthening effects, while β'' precipitates have the best strengthening effects with respect to unit number density. The GP zones have middle strengthening effects.
4. A new parameter, normalized Mg:Si ratio, was defined, and the normalized average Mg:Si ratios of the solute atom clusters and GP zones are near 1 in all samples. The actual Mg:Si ratios of β'' precipitate increase from 1.3 to 1.5 at aging for 2 hours and then remain steady during prolonged aging.

ACKNOWLEDGMENTS

This work was supported by the National Key Research Project and Development Program of China (Grant No. 2016YFB0700401) and the National Natural Science Foundation of China (Grant No. 51301103).

REFERENCES

1. P.N. Rao, B. Viswanadh, and R. Jayaganthan: *Mater. Sci. Eng. A*, 2014, vol. 606, pp. 1–10.
2. C. Cayron and P.A. Buffat: *Acta Mater.*, 2000, vol. 48, pp. 2639–53.
3. S. Pogatscher, H. Antrekowitsch, H. Leitner, T. Ebner, and P.J. Uggowitzer: *Acta Mater.*, 2011, vol. 59, pp. 3352–63.
4. L.F. Cao, P.A. Rometsch, and M.J. Couper: *Mater. Sci. Eng. A*, 2013, vol. 559, pp. 257–61.
5. M. Murayama and K. Hono: *Acta Mater.*, 1999, vol. 47, pp. 1537–48.
6. J. Buha, R.N. Lumley, A.G. Crosky, and K. Hono: *Acta Mater.*, 2007, vol. 55, pp. 3015–24.
7. G.A. Edwards, K. Stiller, G.L. Dunlop, and M.J. Couper: *Acta Mater.*, 1998, vol. 46, pp. 3893–3904.
8. C.S.T. Chang, I. Wieler, N. Wanderka, and J. Banhart: *Ultramicroscopy*, 2009, vol. 109, pp. 585–92.
9. S. Pogatscher, H. Antrekowitsch, H. Leitner, A.S. Sologubenko, and P.J. Uggowitzer: *Scripta Mater.*, 2013, vol. 68, pp. 158–61.
10. R.K.W. Marceau, G. Sha, R. Ferragut, A. Dupasquier, and S.P. Ringer: *Acta Mater.*, 2010, vol. 58, pp. 4923–39.
11. A. Serizawa, S. Hirosawa, and T. Sato: *Metall. Mater. Trans. A*, 2008, vol. 39A, pp. 243–51.
12. E. Clouet, L. Lae, T. Epicier, W. Lefebvre, M. Nastar, and A. Deschamps: *Nat. Mater.*, 2006, vol. 5, pp. 482–88.
13. G. Sha, H. Moller, W.E. Stumpf, J.H. Xia, G. Govender, and S.P. Ringer: *Acta Mater.*, 2012, vol. 60, pp. 692–701.
14. A.K. Gupta, D.J. Lloyd, and S.A. Court: *Mater. Sci. Eng. A*, 2001, vol. 316, pp. 11–17.
15. S.J. Andersen, H.W. Zandbergen, J. Jansen, C. Træholt, U. Tundal, and O. Reiso: *Acta Mater.*, 1998, vol. 46, pp. 3283–98.
16. H.W. Zandbergen, S.J. Andersen, and J. Jansen: *Science*, 1997, vol. 277, pp. 1221–15.
17. H.S. Hasting, A.G. Frøseth, S.J. Andersen, R. Vissers, J.C. Walmsley, and C.D. Marioara: *J. Appl. Phys.*, 2009, vol. 106, p. 123527.
18. W.F. Miao and D.E. Laughlin: *Metall. Mater. Trans. A*, 2000, vol. 31A, pp. 361–71.
19. R. Vissers, M.A. Van Huis, and J. Janden: *Acta Mater.*, 2007, vol. 55, pp. 3815–23.
20. M. Torsæter, W. Lefebvre, C.D. Marioara, S.J. Andersen, J.C. Walmsley, and R. Holmestad: *Scripta Mater.*, 2011, vol. 64, pp. 817–20.
21. M.K. Miller: *Atom Probe Tomography: Analysis at the Atomic Level*, 1st ed., Kluwer Academic/Plenum Publishers, New York, 1999, p. 33.
22. Z.Q. Zheng, W.Q. Liu, Z.Q. Liao, S.P. Ringer, and G. Sha: *Acta Mater.*, 2013, vol. 61, pp. 3724–34.
23. M. Torsæter, H.S. Hasting, W. Lefebvre, C.D. Marioara, J.C. Walmsley, S.J. Andersen, and R. Holmestad: *J. Appl. Phys.*, 2010, vol. 108, p. 073527.
24. J. Buha, R.N. Lumley, and A.G. Crosky: *Phil. Mag.*, 2008, vol. 88, pp. 373–90.
25. B. Gault, M.P. Moody, J.M. Cairney, and S.P. Ringer: *Atom Probe Microscopy*, Springer, New York, 2012.
26. A. Kelly and R.B. Nicholson: *Progr. Mater. Sci.*, 1963, vol. 10, pp. 149–391.
27. P. Haasen: in *Materials Science and Technology*, R.W. Cahn, P. Haasen, and E.J. Kramer, eds., VCH Publishers, New York, 1991.
28. W.J. Poole, X. Wang, D.J. Lloyd, and J.D. Embury: *Phil. Mag.*, 2005, vol. 85, pp. 3113–35.
29. A. Serizawa, T. Sato, and W.J. Poole: *Phil. Mag. Lett.*, 2010, vol. 90, pp. 279–87.
30. M.J. Starink, L.F. Cao, and P.A. Rometsch: *Acta Mater.*, 2012, vol. 60, pp. 4194–4207.
31. S. Esmaeili and D.J. Lloyd: *Acta Mater.*, 2005, vol. 53, pp. 5257–71.